ACS Catalysis

Article

Fully Conjugated Donor-Acceptor Covalent Organic Frameworks for Photocatalytic Oxidative Amine Coupling and Thioamide Cyclization

Shuai Li, Li Li, Yijun Li, Lu Dai, Caixia Liu, Yanze Liu, Jiani Li, Jianning Lv, Pengfei Li, and Bo Wang

ACS Catal., **Just Accepted Manuscript** • DOI: 10.1021/acscatal.0c01242 • Publication Date (Web): 10 Jul 2020

is published by the American Chemical Society. 1155 Sixteenth Street N.W., Washington, DC 20036

Fully Conjugated Donor-Acceptor Covalent Organic Frameworks for Photocatalytic Oxidative Amine Coupling and Thioamide Cyclization

Shuai Li,[a] Li Li,[a] Yijun Li,[a] Lu Dai,[a] Caixia Liu,[a] Yanze Liu,[a] Jiani Li,[a] Jianning Lv,[a] Pengfei Li[a] and Bo Wang*[a]*

[a]Key Laboratory of Cluster Science Ministry of Education, Beijing Key Laboratory of Photoelectronic/Electrophotonic, Advanced Research Institute of Multidisciplinary Science, School of Chemistry and Chemical Engineering, Beijing Institute of Technology, Beijing, China 100081.

Abstract

Covalent organic frameworks (COFs) are promising candidates as heterogeneous photocatalysts due to their porosity and tunable light absorption. The photostability and charge separation of covalent organic frameworks are highly important to improve the efficiency of photocatalytic transformation. In this work, a fully conjugated donor-acceptor COF is constructed with benzothiadiazole unit, which exhibits high stability and enhanced charge separation. The prepared COF can efficaciously produce superoxide radical anion under air and visible light, which mediates the photocatalytic oxidative amine coupling and cyclization of thioamide to 1,2,4-

thiadiazole in moderate to high yield and high recyclability (18 examples). This study demonstrates the great capacity of fully conjugated COFs with D-A structure for light-driven organic synthesis.

KEYWORDS: covalent organic frameworks, donor-acceptor, superoxide radical anion, organic synthesis, photocatalysis.

Introduction

Visible-light driven organic transformations offer a highly sustainable and environment friendly route for the synthesis of important chemicals, which have attracted significant attention in recent years.[1-3] Heterogeneous visible-light photocatalysts with great recyclability are especially promising for large scale applications.[4] Inorganic semiconductors with well-defined band structures are intensely investigated as heterogenous photocatalyst, such as TiO_2 and ZnO, which mostly work in the UV range.[5, 6] Subsequently, organic based photocatalysts, such as organic dyes, are developed to enhance the visible light absorption. To further escalate the catalytic performance, porous photocatalyst or porous material supported semiconductors with exposed photocatalytic sites have been synthesized, such as metal organic frameworks,[7, 8] covalent organic frameworks,[9, 10] conjugated microporous polymers[11, 12] and g-C_3N_4.[13] Among these porous materials, COFs are particularly attractive due to their chemical and structural features.

COFs are a class of polymers with high crystallinity and porosity, which are constructed from organic building blocks with well-defined pore structure and highly tunable opto-electronic properties.[14-16] In recent years, COFs have been found a variety of applications, such as gas sorption and separation,[17-20] energy transformation and storage,[21-24] and particularly heterogeneous catalysis.[25-30] 2D COFs are emerging heterogeneous photocatalysts owing to the combination of strong visible light absorption and mesopore structure. Under visible-light irradiation, the photo-generated electrons and holes in COFs promote a series of reactions, such as hydrogen generation,[31-34] oxygen evolution,[35-37] carbon dioxide reduction[38-40] and organic transformations.[41-53] To obtain higher photocatalytic efficiency, enhanced light absorption, suitable band positions, and fast charge separation are highly important. All these properties are related to the intrinsic chemical linkage of particular COFs. Among many different linkages, the construction of fully conjugated covalent organic frameworks would realize desirable light absorption and charge separation. Until very recently, several ethylene-linked COFs have been synthesized and applied to fluorescence,[54, 55] lithium-ion battery,[56] supercapacitor[57] and others.[58-60] Only a few reports investigate the photocatalytic performance of fully conjugated COFs. Jiang's group reported a 2D vinylene-linked COF that shows impressive photocatalytic hydrogen production activity.[61] Zhang's group introduced pyridine and triazine cores into olefin-based COFs, which grant them strong light-harvesting characteristics and further improved their photocatalytic hydrogen evolution rate.[62, 63] Wang and co-workers incorporated porphyrin to a 2D vinylene-linked COF, which shows good photocatalytic activity of oxidative secondary amine to imine due to improved

photo-stability and enhanced electron delocalization.[64] Li and co-workers introduced nitrogen atom in the skeleton of TP-COF to modulate its electronic structure and lead to a good simulation of artificial photosystem I.[65] Recently, Cooper's group synthesized a bipyridine-containing sp^2c-COF modified with a rhenium complex to improve photocatalytic carbon dioxide reduction performance.[66] Fast charge separation in these fully conjugated COFs is very important and can further improve their photocatalytic performance. The incorporation of donor-acceptor moieties in porous organic systems has been demonstrated to be an effective way to promote the charge seperation.[67, 68] Herein, we designed and synthesized a fully conjugated Py-BSZ-COF, containing electron-donating pyrene unit and electron-accepting benzothiadiazole unit to construct a donor-acceptor structure, which shows high photo-stability and enhanced charge separation. Under visible light irradiation, this D-A Py-BSZ-COF can produce superoxide radical anion ($O_2^{\bullet-}$) in air saturated CH_3CN, which drives the photocatalytic oxidative amine coupling and cyclization of thioamide to 1,2,4-thiadiazole in moderate to high yield and high recyclability.

Experimental Section

The preparation of COFs

Py-BSZ-COF: 1,3,6,8-tetrakis(4-formylphenyl)pyrene (20 mg, 0.032 mmol) and 4,4'-(benzothiadiazole-4,7-diyl)diacetonitrile (24 mg, 0.065 mmol) in 2 mL *o*-dichlorobenzene were added to a 10 mL Pyrex tube. After sonification, 0.2 mL of 1 M tetrabutylammonium hydroxide

(TBAH) in methanol and 0.1 mL water were added. After three freeze-thaw cycles, the tube was flame-sealed and heated at 120 °C for 72 h. The precipitate was washed by DMF, 1 M HCl aqueous solution, water and THF, successively. The solid was Soxhlet extracted with THF for 24 h and activated at 120 °C under vacuum for 12 h to afford an orange powder of 34 mg in 81% yield. Elemental analysis showed that the weight percentage of C, H, N and S to be 74.2%, 3.7%, 7.7% and 4.84%, which is in well agreement with the calculated value of Py-BSZ-COF ($C_{44}H_{23}N_4S$, C 82.6%, H 3.6%, N 8.8%, S 5.0%).

COF-JLU22 was prepared according to the literature method.[44] After activation at 120 °C under vacuum, a red powder of COF-JLU22 was obtained in 76% yield.

sp²c-COF-3 was prepared according to the literature method.[54] After activation at 120 °C under vacuum, an orange powder of sp²c-COF-3 was obtained in 75% yield.

Electrochemical measurements

COF powder (6 mg) was ground with poly(vinylidene fluoride) (PVDF, 2 mg), then ultrasonically dispersed in 2 mL of acetone. The resultant slurry was then drop-casted onto indium tin oxide (ITO) glass with an area of 0.5 × 0.5 cm^2. A Pt wire (counter electrode), a Ag/AgCl electrode (reference electrode), and a coated ITO conductive glass (working electrode) were assembled into a three-electrode system with 0.2 M Na_2SO_4 aqueous solution was used as the electrolyte. The Mott-Schottky plots were collected in dark at different frequencies. The photocurrent measurements

were conducted under the irradiation of a 300 W xenon lamp (100 mW cm^{-1}) with a 420 nm cut-off filter under a nitrogen or oxygen saturated atmosphere. For cyclic voltammetry (CV) tests, the working electrode was prepared by dropping the prepared suspension onto a glassy carbon electrode, then CV experiments were carried on a three-electrode system (saturated calomel electrode as the reference electrode, platinum wire as the counter electrode, glassy carbon electrode as the working electrode) in nitrogen saturated 0.1 M tetrabutylammonium hexafluorophosphate acetonitrile solution with a scan rate of 50 mV s^{-1}.

To investigate the possible influence of the Pt diffusion, all the electrochemical tests were conducted by using a graphite rod as the counter electrode under the same experimental conditions.

Electron spin resonance (ESR) measurements

ESR experiments were conducted in a mixture of 1 mg mL^{-1} Py-BSZ-COF and 0.1 M DMPO air-saturated acetonitrile suspension in dark or irradiated by 300 W xenon lamp (100 mW cm^{-1}) with a 420 nm cut-off filter.

Results and Discussion

The highly crystalline Py-BSZ-COF was obtained by the condensation of 1,3,6,8-tetrakis(4-formylphenyl)pyrene (Py-4CHO) and 4,4'-(benzothiadiazole-4,7-diyl)diacetonitrile (BSZ-2CN) in a mixture of *o*-dichlorobenzene and 1 M TBAH at 120 °C for 72 h, which afforded an orange

powder in 81% yield (Figure 1). The chemical structure of Py-BSZ-COF was first demonstrated by the existence of C=C–H and C≡N stretching bands at around 3030 cm^{-1} and 2214 cm^{-1} and the attenuation of the C=O stretching band at 1697 cm^{-1} in Fourier transform infrared (FT-IR) spectrum (Figure 2a). A broad peak with several close shoulders from 120 to 140 ppm can be assigned to the aromatic carbons and ethylene carbons of Py-BSZ-COF in ^{13}C CP-MAS NMR spectrum. A weak carboxylic carbon at ~180 ppm could be observed, which is due to the partially oxidation of the residue aldehyde groups in the COF (Figure S1).

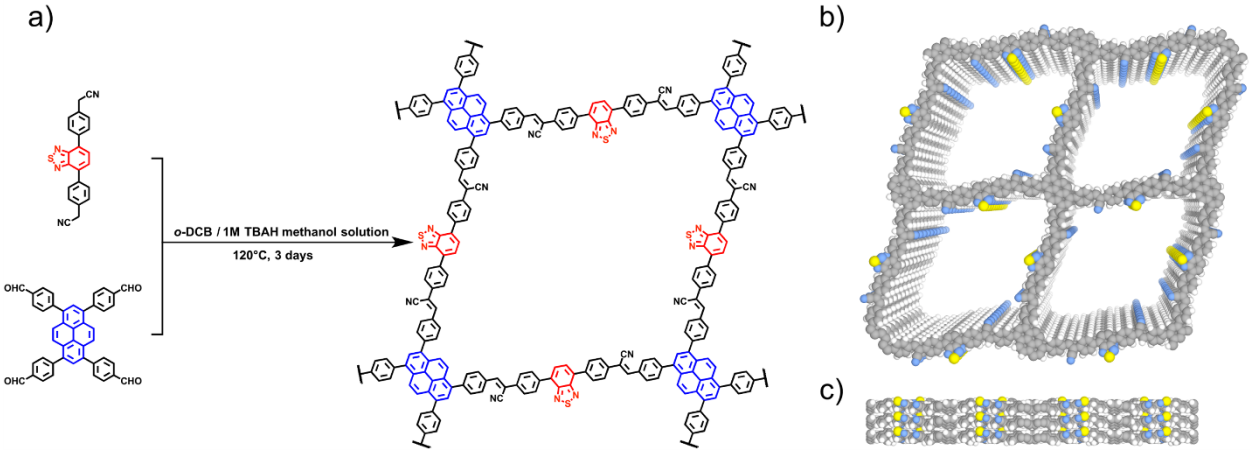

Figure 1. a) The synthetic condition of Py-BSZ-COF. b) Top and c) side views of the structural model of Py-BSZ-COF (C, gray; N, blue; S, yellow; H, white).

The PXRD pattern revealed that Py-BSZ-COF is highly crystalline with diffraction peaks at 2.7°, 5.5°, 8.3°, 11.1° and 24.0°, which are assignable to (110), (220), (400), (440) and (001) facets, respectively. Structural models with AA and AB stacking were constructed by Materials Studio (Figure 1 and S2). The simulated PXRD pattern of the eclipsed AA stacking model was in good

agreement with the experimental PXRD, while the AB stacking model did not (Figure 2b). In addition, the Pawley refinement was performed on the experimental PXRD pattern of Py-BSZ-COF, which resulted in cell unit parameters of a = 51.3 Å, b = 42.5 Å, c = 3.8 Å, and $\alpha = \gamma = 90^{o}$, $\beta = 96.6^{o}$ with a negligible difference of R_{wp} = 3.70% and R_p = 2.86%.

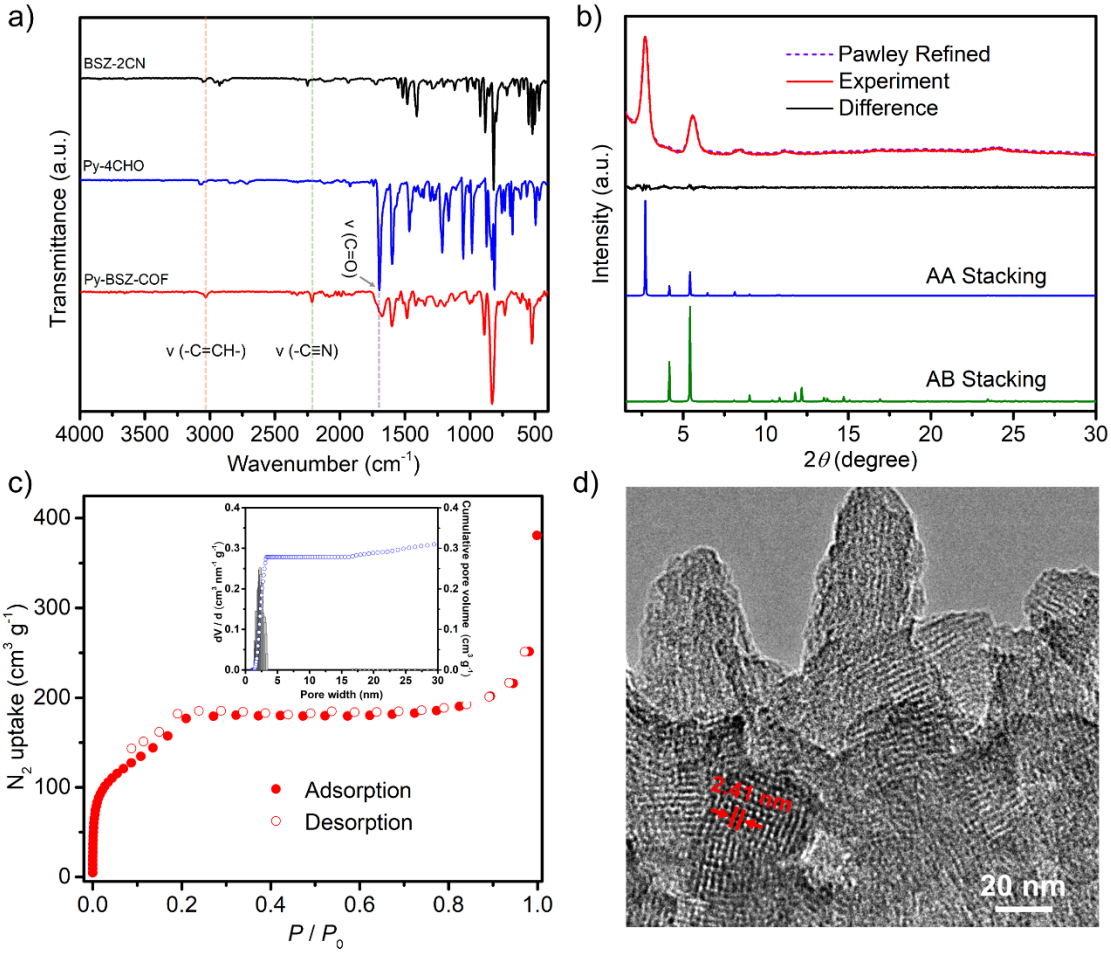

Figure 2. a) FT-IR spectra of Py-BSZ-COF, BSZ-2CN and Py-4CHO. b) Experimentally observed PXRD pattern, Pawley refinement and their difference of Py-BSZ-COF (red, purple dots, black), the simulated PXRD patterns of the AA stacking model (blue) and the AB stacking model (green).

c) N_2 isotherm of Py-BSZ-COF at 77 K, inset: pore width distribution and cumulative pore volume of Py-BSZ-COF. d) HR-TEM image of Py-BSZ-COF.

The porosity of Py-BSZ-COF was investigated by the N_2 adsorption isotherm at 77 K (Figure 2c). The Brunauer–Emmett–Teller (BET) surface area was evaluated to be 600 m^2 g^{-1} with a total pore volume of 0.33 cm^3 g^{-1} at P/P_0 = 0.98. The pore size of Py-BSZ-COF was estimated to be 2.4 nm by nonlinear density functional theory (NLDFT), which consists well with pore width predicted by the structural model. Scanning electron microscopy (SEM) and transmission electron microscopy (TEM) images show that Py-BSZ-COF has a belt-like morphology (Figure S3 and S4). High resolution transmission electron microscopy (HR-TEM) of Py-BSZ-COF reveals a clear lattice fringe of 2.41 nm, which is close to the pore size calculated from the nitrogen isotherm (Figure 2d). In addition, the energy dispersive spectroscopy (EDS) mapping of Py-BSZ-COF shows a homogeneous distribution of carbon, nitrogen and sulfur elements in the particles (Figure S5).

Due to the irreversible nature of ethylene linkage, Py-BSZ-COF offers high thermal-, chemical- and photo- stability, which is stable over 400 °C and remains crystallinity, structural intact and porosity after immerse in 12 M HCl, 12 M NaOH and boiling water or illuminate under 15 W white LED bulb in a CH_3CN suspension for at least 3 days as determined by the comparison of the PXRD patterns, FT-IR spectra and N_2 isotherm at 77 K before and after the treatments (Figure S6–S9). The high stability of Py-BSZ-COF makes it a promising candidate in photocatalysis.

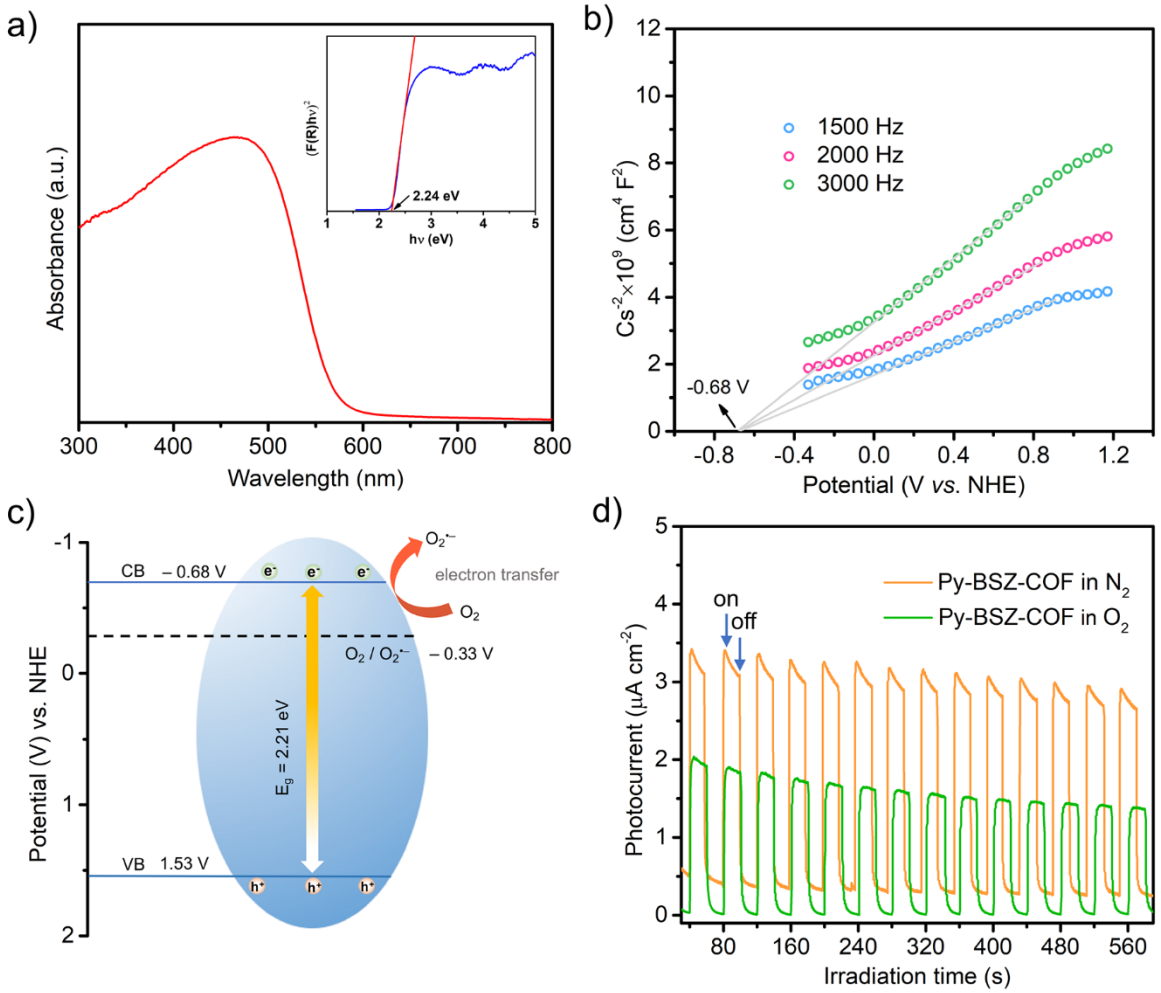

Figure 3. a) Solid state UV–vis diffuse reflectance spectra (red), inset: Tauc plot of Py-BSZ-COF (blue). b) The Mott-Schottky plots of Py-BSZ-COF. c) The band energy diagram of Py-BSZ-COF. d) Photocurrent responses spectra of Py-BSZ-COF under nitrogen or oxygen atmosphere.

The UV–vis diffuse reflection spectrum of Py-BSZ-COF exhibits a broad visible adsorption range up to 600 nm. The optical band gap of Py-BSZ-COF is calculated to be 2.24 eV by using the Tauc plot (Figure 3a). The cyclic voltammetry of Py-BSZ-COF shows a reversible half wave potential ($E_{1/2}$) at 1.47 V *vs*. NHE (Figure S10), which can be assigned to the Py-BSZ-COF^{+}/Py-BSZ-COF

couple. To determine the positions of the conduction band (CB) and valence band (VB), the electrochemical Mott-Schottky spectra and VB X-ray photoelectron spectroscopy (VB-XPS) of Py-BSZ-COF were measured. The Mott-Schottky plot of Py-BSZ-COF has a positive slope, which suggests an n-type semiconductor behavior. For an n-type semiconductor, the CB position is close to its flat band potential.[69] Therefore, the CB position of Py-BSZ-COF is estimated to be –0.68 V *vs*. NHE at pH = 7 (Figure 3b and S11). The VB edge of Py-BSZ-COF is determined by the VB-XPS spectrum, which is located at 1.53 eV (Figure S12). The band gap of Py-BSZ-COF calculated from the Mott-Schottky plots and VB-XPS spectrum is 2.21 eV, which is quite closed to the optical band gap. To rule out the possible of Pt diffusion during the electrochemical experiments, we also tested the cyclic voltammetry, Mott-Schottky spectra of Py-BSZ-COF by using a graphite rod as the counter electrode under the same conditions. The reversible half wave potential ($E_{1/2}$) and CB position of Py-BSZ-COF determined from the graphite counter electrode are quite close to that of the Pt electrode, which are 1.45 V and –0.67 V *vs*. NHE at pH = 7, respectively (Figure S10 and S11). Combine all the evidence, the CB of Py-BSZ-COF (–0.68 V *vs*. NHE) is negative than the potential required for the reduction of O_2 to superoxide radical (–0.33 V *vs*. NHE), which makes Py-BSZ-COF a potential photocatalyst in generating critical superoxide radical ($O_2^{\bullet-}$) intermediate (Figure 3c). The photo-generation of superoxide radical in solution with Py-BSZ-COF was probed by electron spin resonance (ESR) spectra. Upon light irradiation of Py-BSZ-COF with 5,5-dimethyl-1-pyrroline-*N*-oxide (DMPO) in an air-saturated CH_3CN, the intensity of the characteristic peaks of typical DMPO–$O_2^{\bullet-}$ adduct were increased by prolonging the illumination

time (Figure S13). The existence of $O_2^{\bullet-}$ in an irradiated Py-BSZ-COF suspension is also confirmed by the reduction of a yellow colored nitro blue tetrazorium (Figure S14).[70] In addition, the transient photocurrent responses of Py-BSZ-COF over several on-off photoirradiation cycles show high photo-induced charge separation under both nitrogen and oxygen atmosphere. The photocurrent of Py-BSZ-COF under nitrogen is higher than that under oxygen atmosphere, which could arise from the quenching of the photo-generated electrons by oxygen to generate superoxide radical anion. (Figure 3d and S15).

Table 1. Control experiments of the photocatalytic oxidative amine coupling of benzylamine.[a]

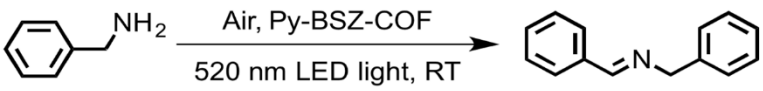

Entry	Reaction condition variations	Light	Conversion[b](%)
1	–	on	99
2[c]	–	off	4
3[d]	no O_2	on	9
4	no photocatalyst	on	5
5[e]	L-histidine	on	94
6[f]	catalase	on	96
7[g]	isopropanol	on	95
8[h]	*p*-benzoquinone	on	28
9[i]	$AgNO_3$	on	1
10[j]	KI	on	38
11	sp^2c-COF-3	on	67
12	COF-JLU22	on	90[k]

[a] Reaction conditions: benzylamine (0.2 mmol), photocatalyst (5 mg), 2 mL CH_3CN, 1 atm air, 12 h and 15 W 520 nm LED bulb (5 mW cm^{-2}). [b] Determined by ^1H NMR spectroscopic analysis. [c] In the dark. [d] Under Ar environment. [e] L-histidine used as $^1O_2$ radical scavenger. [f] Catalase used as H_2O_2 scavenger. [g] Isopropanol used as •OH radical scavenger. [h] *p*-benzoquinone used as $O_2^{\bullet-}$ radical scavenger. [i] $AgNO_3$ used as electron scavenger. [j] KI used as hole scavenger. [k] Partly decomposed during the photocatalysis.

Oxidative amine coupling

Imines are important intermediates in organic synthesis and widely used to synthesize dyes, drugs, and agrochemicals.[71] The direct synthesis of imine from amine under photocatalytic condition has attracted great attention in recent years.[72-75] Considering the significant superoxide radical generating ability and the ideal band gap, the activated Py-BSZ-COF was first tested for the oxidative amine coupling reaction by using benzylamine as the substrate to optimize the reaction condition. When benzylamine (0.2 mmol) and Py-BSZ-COF (5 mg) in 2 mL of CH_3CN was irradiated over a 15 W 520 nm LED bulb (5 mW cm^{-2}) under air at room temperature, the formation of *N*-benzyl-1-phenylmethanimine was observed with 99% conversion (Table 1, entry 1). A series of control experiments demonstrated that the photocatalyst Py-BSZ-COF, oxygen and light are all indispensable reaction conditions, otherwise little or trace conversion can be observed (Table 1, entries 2–4). To determine the key intermediate in the photocatalytic transformation, a series of trapping agents with different quenching targets has been added to the reaction mixture. The

addition of L-histidine (L-His), catalase (CAT) and isopropanol (IPA) shows negligible decrease of the reaction yield, which rules out the existence of $^1O_2$, H_2O_2 and •OH during the photocatalysis (Table 1, entries 5–7). After adding *p*-benzoquinone (Bq), a typical $O_2^{\bullet-}$ scavenger, the reaction yield was significantly reduced from 99% to 28%. These quenching experiments suggest that $O_2^{\bullet-}$ is the predominant radical in this reaction (Table 1, entry 8). The addition of $AgNO_3$ can fully quench photo-generated electrons, which completely inhibits the reaction (Table 1, entry 9). Furthermore, by using KI as the hole scavenger, only 38% of benzylamine converted to the corresponding imine, which indicated the photo-generated holes are also important in the amine coupling reaction (Table 1, entry 10).

To study the donor and acceptor behavior of Py-BSZ-COF, two iso-reticular COFs with benzothiazole in the imine linked COF-JLU22 and without benzothiazole in the olefin bridged sp^2c-COF-3 were synthesized and fully characterized (Figure S16–S25). The UV-vis diffuse reflection spectrum of Py-BSZ-COF is significantly red-shifted as compared to sp^2c-COF-3 with maximum absorption and absorption onset quite close to the benzothiazole incorporated COF-JLU22 (Figure S26 and S27). Photoluminescence (PL) spectra reveal a weaker fluorescence intensity of Py-BSZ-COF as compared to sp^2c-COF-3 and COF-JLU22 (Figure S28). Time-resolved PL spectra demonstrate a longer fluorescence lifetime of Py-BSZ-COF (1.6 ns) as compared with sp^2c-COF-3 (1.2 ns) and COF-JLU22 (1.1 ns). The weaker PL emission and longer fluorescence lifetime of Py-BSZ COF clearly demonstrated that the recombination of photo-

generated excitons was inhibited (Figure S29). In addition, the introduction of benzothiazole in the fully conjugated Py-BSZ-COF provides an improved charge separation, which generates higher transient photocurrent responses compared to both sp^2c-COF-3 and COF-JLU22 under nitrogen or oxygen atmosphere (Figure S30 and S31). Similarly, the photocurrent responses were also conducted with a graphite counter electrode to eliminate the possible influence of Pt electrode. The photocurrents of Py-BSZ-COF are higher than sp^2c-COF-3 and COF-JLU22 under both nitrogen and oxygen atmosphere. All three COFs also exhibit decreased photocurrents under oxygen atmosphere, which were in accordance with the results by using a Pt electrode (Figure S15b, S30b and S31b). As a result, the iso-reticular sp^2c-COF-3 only affords a moderate yield of 67% (Table 1, entry 11). Similar D-A structure in an imine linked COF-JLU22 has a comparable yield with the Py-BSZ-COF (Table 1, entry 12). However, COF-JLU22 partly decomposed in the process of photocatalysis due to the dynamic imine exchange between COF-JLU22 and benzylamine, and the exchange product was observed in ^{1}H NMR (Figure S32).

With the optimal photocatalyst, we expand the substrate scope to various benzylamine with different functional groups. High conversion (> 99%) and selectivity (> 98%) were obtained for 4-substituted benzylamine with electron donating groups such as Me-, MeO- and electron withdrawing groups like F-, Cl-, Br-, CF_3- and CN- (Table 2). CN- in 4-substituted benzylamine slows down the reaction rate and lowers the conversion, which may due to the strong electron-withdrawing effect of the cyano group in destabilizing the cationic radical intermediate.[76] The

conversion of 4-cyanobenzylamine to **2h** can increase from 52% to 84% by prolonging the reaction time to 24 h. Moreover, heterocyclic amine like 2-thiophenemethanamine can completely convert to imine **2i** in nearly quantitative yield. The Py-BSZ-COF catalyst has a high recyclability with conversion and selectivity both over 98% after four consecutive runs (Figure S33 and S34). The PXRD and FT-IR spectra of Py-BSZ-COF after three cycles remain the same as the pristine one, which suggest high photostability of Py-BSZ-COF during the catalysis (Figure S35).

Table 2. Heterogeneous photocatalytic oxidative coupling of diverse amines.[a]

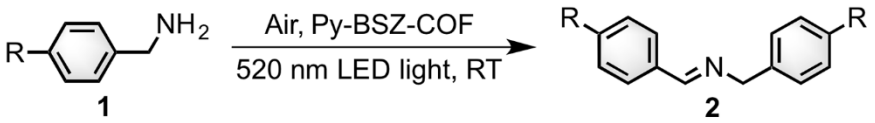

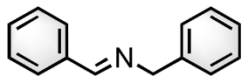

2a

12 h, 99%, 99%

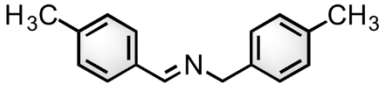

2b

12 h, 99%, 99%

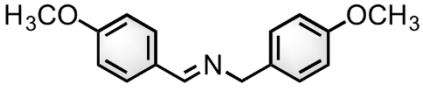

2c

12 h, 98%, 99%

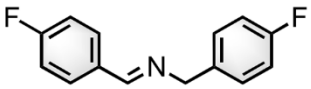

2d

12 h, 99%, 99%

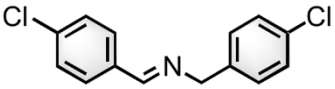

2e

12 h, 99%, 99%

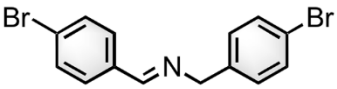

2f

12 h, 99%, 99%

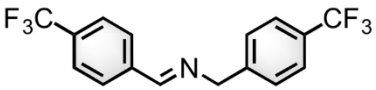

2g

12 h, 98%, 98%

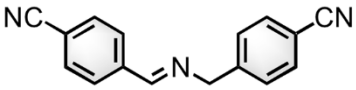

2h

12 h, 52%, 99%

24 h, 84%, 99%

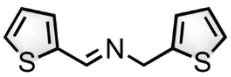

2i

12 h, 67%, 99%

24 h, 99%, 99%

[a] Reaction conditions: amine (0.2 mmol), photocatalyst (5 mg), 2 mL CH_3CN, 1 atm air and 15 W 520 nm LED bulb (5 mW cm^{-2}). Conversion (red) and selectivity (blue) are determined by ^1H NMR spectroscopic analysis.

Oxidative cyclization of thioamide to 1,2,4-thiadiazole

Compounds containing 1,2,4-thiadiazole are biologically and pharmaceutically important.[77] Pharmaceuticals with 1,2,4-thiadiazole as the key scaffold exhibit promising activity in suppressing inflammation, central nervous system activity and antibiotic action, such as the most famous commercially available antibiotic cefozopram.[78] Most of the synthetic routes available for 1,2,4-thiadiazoles rely on the oxidative cyclization of thioamides by various oxidants such as DDQ,[79] iodate[80] and phosphovanadomolybdic acid.[81] Here, Py-BSZ-COF was explored as a photocatalyst to oxidative cyclization of thioamide due to its outstanding capability to generate $O_2^{\bullet-}$. When the thioamide (0.4 mmol) and catalytic amount of Py-BSZ-COF (10 mg) in 4 mL of DMF was illuminated with a 15 W white LED bulb (11 mW cm^{-2}) under air at room temperature, 3,5-diphenyl-1,2,4-thiadiazole was obtained in 90% yield (Table 3, entry 1). Control experiments showed that the light, oxygen, and Py-BSZ-COF are all essential (Table S1, entries 2–4). In addition, radical scavenger experiments suggest that $O_2^{\bullet-}$ is also the predominant radical in the oxidative cyclization of thioamide (Table S1, entries 5-8). A variety of thioamides can be converted to 1,2,4-thiadiazoles in moderate to good yield under mild condition. The oxidative cyclization of thioamides with electron donating groups like Me- and MeO- provides good yields

over 87%, while the electron withdrawing groups lead to a slightly lower yield (Table 3). Heterocyclic thioamide like 2-thiophenecarboxamide can also be cyclized in satisfying yield of 84%. The recyclability of Py-BSZ-COF in oxidative cyclization of thioamide was also tested in four consecutive cycles, after which the isolated yield of 3,5-diphenyl-1,2,4-thiadiazole reduced slightly from 90% to 84% possibly due to the loss of photocatalyst during the recycling experiments (Figure S28). Same as in the photocatalytic amine coupling, Py-BSZ-COF also exhibits high photostability in the oxidative cyclization of thioamide as the PXRD and FT-IR spectra of Py-BSZ-COF remain unchanged after three reuses (Figure S36).

Table 3. Heterogeneous photocatalytic oxidative cyclization of diverse thioamides to 1,2,4-thiadiazoles.[a]

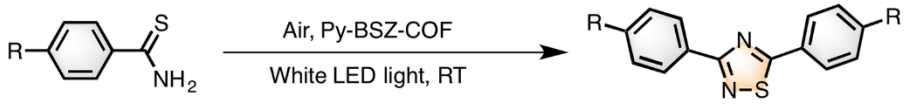

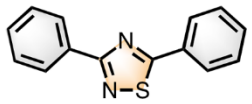

4a
12 h, 90%

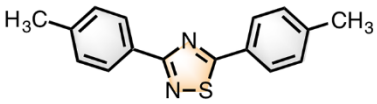

4b
18 h, 87%

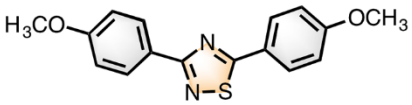

4c
20 h, 91%

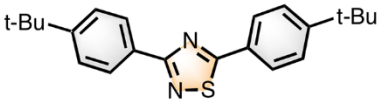

4d
48 h, 64%

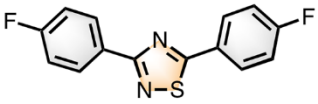

4e
30 h, 76%

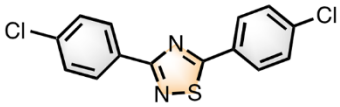

4f
24 h, 82%

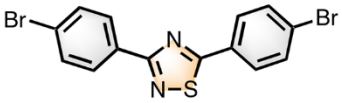

4g
30 h, 78%

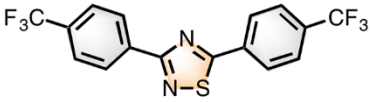

4h
48 h, 56%

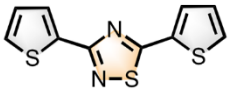

4i
24 h, 84%

[a] Reaction conditions: thioamide (0.4 mmol), photocatalyst (10 mg), 4 mL DMF, 1 atm air, and 15 W white LED bulb (11 mW cm^{-2}). Isolated yield after chromatography over silica.

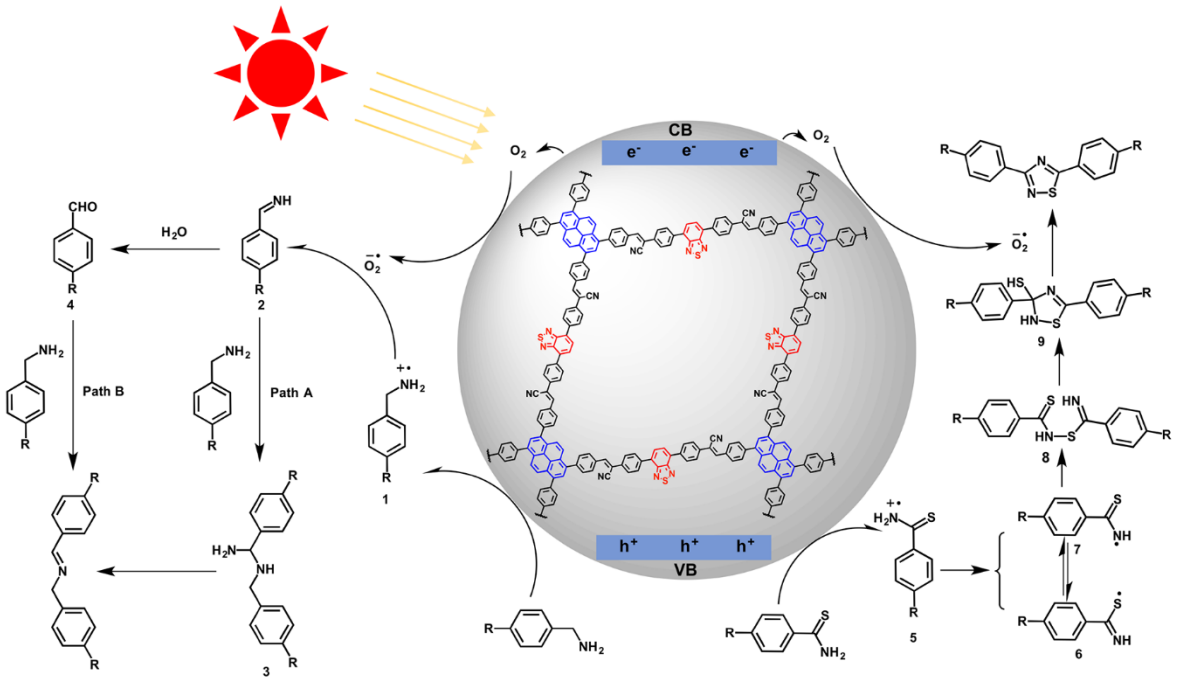

Figure 4. The plausible photocatalytic mechanisms of Py-BSZ-COF mediated oxidative amine coupling and cyclization of thioamide to 1,2,4-thiadiazole.

Reaction mechanism

Based on the above experiments and literature reports,[72, 82-87] tentative reaction mechanisms for the oxidative amine coupling and cyclization of thioamide to 1,2,4-thiadiazole were proposed (Figure 4). Py-BSZ-COF is first photo-excited to Py-BSZ-COF* under visible light. The photo-generated electrons in Py-BSZ-COF* reduce molecular oxygens to superoxide radicals. At the same time, the resulted Py-BSZ-COF^{+} oxidizes amine to amine radical anion **1** and regenerates the Py-BSZ-COF. The $O_2^{\bullet-}$ abstracts a H^{+} and a hydrogen atom from **1** to give the key intermediate phenylmethanimine **2**. After that, two paths are possible. In path A, intermediate **2** is attacked by

another molecule of benzylamine to give an aminal **3**. After the loss of NH_3, the final product *N*-benzyl-1-phenylmethanimine is produced. In path B, intermediate **2** is hydrolyzed to afford the benzaldehyde **4**, which subsequently condensed with another molecule of amine to yield the final product. We could detect the existence of benzaldehyde **4** with gas chromatography/mass spectrometer (GC/MS), thus path B is more likely to happen in our system (Figure S37). Similarly, the Py-BSZ-COF$^+$ could also oxidize thioamide to a thioamide radical cation **5**. Two radical isomers **6** and **7** are formed with the proton removal and linked to give a dimer **8**. The final 1,2,4-thiadiazole was obtained through the intramolecular cyclization of dimer **8** and aromatization of **9** with the help of superoxide radical anion.

Conclusion

A benzothiazole-containing D-A covalent organic framework with fully conjugated ethylene linkage was designed and synthesized in high crystallinity and high yield. The introduction of benzothiazole to the framework induces the red-shift of the visible light absorption and the fast separation of photo-generated charges. The resultant D-A Py-BSZ-COF can produce superoxide radical anion ($O_2^{\bullet-}$) for the photocatalytic oxidative amine coupling and cyclization of thioamide to 1,2,4-thiadiazole with broad substrate scope, good yield and high recyclability.

AUTHOR INFORMATION

Corresponding Author

* lipengfei@bit.edu.cn

* bowang@bit.edu.cn

Author Contributions

The manuscript was written through contributions of all authors. All authors have given approval to the final version of the manuscript.

ASSOCIATED CONTENT

Supporting Information

This information is available free of charge on the ACS Publication website.

Materials and instruments; Synthesis of monomers; Characterizations of COFs; Photocatalytic procedures and cycle performance of aerobic oxidation coupling of benzylamine and oxidative cyclization of thioamide; ^{1}H and ^{13}C NMR spectra of monomers and reaction products. (PDF)

ACKNOWLEDGMENT

The financial support from the National Natural Science Foundation of China (No. 81601549, 61933002, 21674012 and 21625102); the 1000 Plan (Youth); Beijing Municipal Science and Technology Project (Z181100004418001), Beijing Institute of Technology Research Fund

Program for Young Scholars is acknowledged. The authors acknowledge the Analysis and Testing Center of BIT for technical supports.

REFERENCES

1. Marzo, L.; Pagire, S. K.; Reiser, O.; Konig, B. Visible-Light Photocatalysis: Does It Make a Difference in Organic Synthesis? *Angew. Chem., Int. Ed.* **2018,** *57*, 10034–10072.

2. Douglas, J. J.; Sevrin, M. J.; Stephenson, C. R. J. Visible Light Photocatalysis: Applications and New Disconnections in the Synthesis of Pharmaceutical Agents. *Org. Process Res. Dev.* **2016,** *20*, 1134–1147.

3. Schultz, D. M.; Yoon, T. P. Solar Synthesis: Prospects in Visible Light Photocatalysis. *Science* **2014,** *343*, No. eeal1239176.

4. Lang, X. J.; Chen, X. D.; Zhao, J. C. Heterogeneous Visible Light Photocatalysis for Selective Organic Transformations. *Chem. Soc. Rev.* **2014,** *43*, 473–486.

5. Asahi, R.; Morikawa, T.; Irie, H.; Ohwaki, T. Nitrogen-Doped Titanium Dioxide as Visible-Light-Sensitive Photocatalyst: Designs, Developments, and Prospects. *Chem. Rev.* **2014,** *114*, 9824–9852.

6. Ong, C. B.; Ng, L. Y.; Mohammad, A. W. A Review of ZnO Nanoparticles as Solar Photocatalysts: Synthesis, Mechanisms and Applications. *Renewable Sustainable Energy Rev.* **2018,** *81*, 536–551.

7. Xiao, J. D.; Jiang, H. L. Metal-Organic Frameworks for Photocatalysis and Photothermal Catalysis. *Acc. Chem. Res.* **2019,** *52*, 356–366.

8. Zhang, T.; Lin, W. B. Metal-Organic Frameworks for Artificial Photosynthesis and Photocatalysis. *Chem. Soc. Rev.* **2014,** *43*, 5982–5993.

9. Banerjee, T.; Gottschling, K.; Savasci, G.; Ochsenfeld, C.; Lotsch, B. V. H_2 Evolution with Covalent Organic Framework Photocatalysts. *ACS Energy Lett.* **2018,** *3*, 400–409.

10. Stegbauer, L.; Schwinghammer, K.; Lotsch, B. V. A Hydrazone-Based Covalent Organic Framework for Photocatalytic Hydrogen Production. *Chem. Sci.* **2014,** *5*, 2789–2793.

11. Sprick, R. S.; Jiang, J. X.; Bonillo, B.; Ren, S. J.; Ratvijitvech, T.; Guiglion, P.; Zwijnenburg, M. A.; Adams, D. J.; Cooper, A. I. Tunable Organic Photocatalysts for Visible-Light-Driven Hydrogen Evolution. *J. Am. Chem. Soc.* **2015,** *137*, 3265–3270.

12. Chaoui, N.; Trunk, M.; Dawson, R.; Schmidt, J.; Thomas, A. Trends and Challenges for Microporous Polymers. *Chem. Soc. Rev.* **2017,** *46*, 3302–3321.

13. Cao, S.; Low, J.; Yu, J.; Jaroniec, M. Polymeric Photocatalysts Based on Graphitic Carbon Nitride. *Adv. Mater.* **2015,** *27*, 2150–2176.

14. Ding, S. Y.; Wang, W. Covalent Organic Frameworks (COFs): From Design to Applications. *Chem. Soc. Rev.* **2013,** *42*, 548–568.

15. Feng, X.; Ding, X. S.; Jiang, D. L. Covalent Organic Frameworks. *Chem. Soc. Rev.* **2012,** *41*, 6010–6022.

16. Diercks, C. S.; Yaghi, O. M. The Atom, the Molecule, and the Covalent Organic Framework. *Science* **2017,** *355* No. eeal1585.

17. Doonan, C. J.; Tranchemontagne, D. J.; Glover, T. G.; Hunt, J. R.; Yaghi, O. M. Exceptional Ammonia Uptake by a Covalent Organic Framework. *Nat. Chem.* **2010,** *2*, 235–238.

18. Zeng, Y.; Zou, R.; Zhao, Y. Covalent Organic Frameworks for CO_2 Capture. *Adv. Mater.* **2016,** *28*, 2855–2873.

19. Huang, N.; Chen, X.; Krishna, R.; Jiang, D. Two-Dimensional Covalent Organic Frameworks for Carbon Dioxide Capture through Channel-Wall Functionalization. *Angew. Chem., Int. Ed.* **2015,** *54*, 2986–2990.

20. Ying, Y.; Tong, M.; Ning, S.; Ravi, S. K.; Peh, S. B.; Tan, S. C.; Pennycook, S. J.; Zhao, D. Ultrathin Two-Dimensional Membranes Assembled by Ionic Covalent Organic Nanosheets with Reduced Apertures for Gas Separation. *J. Am. Chem. Soc.* **2020,** *142*, 4472–4480.

21. Wang, S.; Wang, Q.; Shao, P.; Han, Y.; Gao, X.; Ma, L.; Yuan, S.; Ma, X.; Zhou, J.; Feng, X.; Wang, B. Exfoliation of Covalent Organic Frameworks into Few-Layer Redox-Active Nanosheets as Cathode Materials for Lithium-Ion Batteries. *J. Am. Chem. Soc.* **2017,** *139*, 4258–4261.

22. DeBlase, C. R.; Silberstein, K. E.; Truong, T. T.; Abruna, H. D.; Dichtel, W. R. β-Ketoenamine-Linked Covalent Organic Frameworks Capable of Pseudocapacitive Energy Storage. *J. Am. Chem. Soc.* **2013,** *135*, 16821–16824.

23. Zhan, X.; Chen, Z.; Zhang, Q. Recent Progress in Two-Dimensional COFs for Energy-Related Applications. *J. Mater. Chem. A* **2017,** *5*, 14463–14479.

24. Halder, A.; Ghosh, M.; Khayum, M. A.; Bera, S.; Addicoat, M.; Sasmal, H. S.; Karak, S.; Kurungot, S.; Banerjee, R. Interlayer Hydrogen-Bonded Covalent Organic Frameworks as High-Performance Supercapacitors. *J. Am. Chem. Soc.* **2018,** *140*, 10941–10945.

25. Ding, S. Y.; Gao, J.; Wang, Q.; Zhang, Y.; Song, W. G.; Su, C. Y.; Wang, W. Construction of Covalent Organic Framework for Catalysis: Pd/COF-LZU1 in Suzuki-Miyaura Coupling Reaction. *J. Am. Chem. Soc.* **2011,** *133*, 19816–19822.

26. Lu, S.; Hu, Y.; Wan, S.; McCaffrey, R.; Jin, Y.; Gu, H.; Zhang, W. Synthesis of Ultrafine and Highly Dispersed Metal Nanoparticles Confined in a Thioether-Containing Covalent Organic Framework and Their Catalytic Applications. *J. Am. Chem. Soc.* **2017,** *139*, 17082–17088.

27. Xu, H.; Gao, J.; Jiang, D. Stable, Crystalline, Porous, Covalent Organic Frameworks as a Platform for Chiral Organocatalysts. *Nat. Chem.* **2015,** *7*, 905–912.

28. Han, X.; Xia, Q.; Huang, J.; Liu, Y.; Tan, C.; Cui, Y. Chiral Covalent Organic Frameworks with High Chemical Stability for Heterogeneous Asymmetric Catalysis. *J. Am. Chem. Soc.* **2017,** *139*, 8693–8697.

29. Sun, Q.; Tang, Y.; Aguila, B.; Wang, S.; Xiao, F. S.; Thallapally, P. K.; Al-Enizi, A. M.; Nafady, A.; Ma, S. Reaction Environment Modification in Covalent Organic Frameworks for Catalytic Performance Enhancement. *Angew. Chem., Int. Ed.* **2019,** *58*, 8670–8675.

30. Li, H.; Pan, Q.; Ma, Y.; Guan, X.; Xue, M.; Fang, Q.; Yan, Y.; Valtchev, V.; Qiu, S. Three-Dimensional Covalent Organic Frameworks with Dual Linkages for Bifunctional Cascade Catalysis. *J. Am. Chem. Soc.* **2016,** *138*, 14783–14788.

31. Pachfule, P.; Acharjya, A.; Roeser, J.; Langenhahn, T.; Schwarze, M.; Schomacker, R.; Thomas, A.; Schmidt, J. Diacetylene Functionalized Covalent Organic Framework (COF) for Photocatalytic Hydrogen Generation. *J. Am. Chem. Soc.* **2018,** *140*, 1423–1427.

32. Wang, K.; Yang, L. M.; Wang, X.; Guo, L.; Cheng, G.; Zhang, C.; Jin, S.; Tan, B.; Cooper, A. Covalent Triazine Frameworks via a Low-Temperature Polycondensation Approach. *Angew. Chem., Int. Ed.* **2017,** *56*, 14149–14153.

33. Wang, X.; Chen, L.; Chong, S. Y.; Little, M. A.; Wu, Y.; Zhu, W.-H.; Clowes, R.; Yan, Y.; Zwijnenburg, M. A.; Sprick, R. S.; Cooper, A. I. Sulfone-Containing Covalent Organic Frameworks for Photocatalytic Hydrogen Evolution from Water. *Nat. Chem.* **2018,** *10*, 1180–1189.

34. Huang, W.; He, Q.; Hu, Y.; Li, Y. Molecular Heterostructures of Covalent Triazine Frameworks for Enhanced Photocatalytic Hydrogen Production. *Angew. Chem., Int. Ed.* **2019,** *58*, 8676–8680.

35. Lan, Z.-A.; Fang, Y.; Zhang, Y.; Wang, X. Photocatalytic Oxygen Evolution from Functional Triazine-Based Polymers with Tunable Band Structures. *Angew. Chem., Int. Ed.* **2018,** *57*, 470–474.

36. Xie, J.; Shevlin, S. A.; Ruan, Q.; Moniz, S. J. A.; Liu, Y.; Liu, X.; Li, Y.; Lau, C. C.; Guo, Z. X.; Tang, J. Efficient Visible Light-Driven Water Oxidation and Proton Reduction by an Ordered Covalent Triazine-Based Framework. *Energy Environ. Sci.* **2018,** *11*, 1617–1624.

37. Wan, Y.; Wang, L.; Xu, H.; Wu, X.; Yang, J. A Simple Molecular Design Strategy for Two-Dimensional Covalent Organic Framework Capable of Visible-Light-Driven Water Splitting. *J. Am. Chem. Soc.* **2020,** *142*, 4508–4516.

38. Lu, M.; Liu, J.; Li, Q.; Zhang, M.; Liu, M.; Wang, J. L.; Yuan, D. Q.; Lan, Y. Q. Rational Design of Crystalline Covalent Organic Frameworks for Efficient CO_2 Photoreduction with H_2O. *Angew. Chem., Int. Ed.* **2019,** *58*, 12392–12397.

39. Yang, S.; Hu, W.; Zhang, X.; He, P.; Pattengale, B.; Liu, C.; Cendejas, M.; Hermans, I.; Zhang, X.; Zhang, J.; Huang, J. 2D Covalent Organic Frameworks as Intrinsic Photocatalysts for Visible Light-Driven CO_2 Reduction. *J. Am. Chem. Soc.* **2018,** *140*, 14614–14618.

40. Zhong, W.; Sa, R.; Li, L.; He, Y.; Li, L.; Bi, J.; Zhuang, Z.; Yu, Y.; Zou, Z. A Covalent Organic Framework Bearing Single Ni Sites as a Synergistic Photocatalyst for Selective Photoreduction of CO_2 to CO. *J. Am. Chem. Soc.* **2019,** *141*, 7615–7621.

41. Bhadra, M.; Kandambeth, S.; Sahoo, M. K.; Addicoat, M.; Balaraman, E.; Banerjee, R. Triazine Functionalized Porous Covalent Organic Framework for Photo-Organocatalytic E-Z Isomerization of Olefins. *J. Am. Chem. Soc.* **2019,** *141*, 6152–6156.

42. Hao, W.; Chen, D.; Li, Y.; Yang, Z.; Xing, G.; Li, J.; Chen, L. Facile Synthesis of Porphyrin Based Covalent Organic Frameworks via an A_2B_2 Monomer for Highly Efficient Heterogeneous Catalysis. *Chem. Mater.* **2019,** *3*, 8100–8105.

43. Huang, W.; Byun, J.; Rorich, I.; Ramanan, C.; Blom, P. W. M.; Lu, H.; Wang, D.; Caire da Silva, L.; Li, R.; Wang, L.; Landfester, K.; Zhang, K. A. I. Asymmetric Covalent Triazine Framework for Enhanced Visible-Light Photoredox Catalysis via Energy Transfer Cascade. *Angew. Chem., Int. Ed.* **2018,** *57*, 8316–8320.

44. Li, Z.; Zhi, Y.; Shao, P.; Xia, H.; Li, G.; Feng, X.; Chen, X.; Shi, Z.; Liu, X. Covalent Organic Framework as an Efficient, Metal-Free, Heterogeneous Photocatalyst for Organic Transformations under Visible Light. *Appl. Catal. B–Environ.* **2019,** *245*, 334–342.

45. Liu, S.; Pan, W.; Wu, S.; Bu, X.; Xin, S.; Yu, J.; Xu, H.; Yang, X. Visible-Light-Induced Tandem Radical Addition–Cyclization of 2-Aryl Phenyl Isocyanides Catalysed by Recyclable Covalent Organic Frameworks. *Green Chemistry* **2019,** *21*, 2905–2910.

46. Liu, W.; Su, Q.; Ju, P.; Guo, B.; Zhou, H.; Li, G.; Wu, Q. A Hydrazone-Based Covalent Organic Framework as an Efficient and Reusable Photocatalyst for the Cross-Dehydrogenative Coupling Reaction of *N*-Aryltetrahydroisoquinolines. *ChemSusChem* **2017,** *10*, 664–669.

47. Pachfule, P.; Acharjya, A.; Roeser, J.; Sivasankaran, R. P.; Ye, M. Y.; Bruckner, A.; Schmidt, J.; Thomas, A. Donor-Acceptor Covalent Organic Frameworks for Visible Light Induced Free Radical Polymerization. *Chem. Sci.* **2019,** *10*, 8316–8322.

48. Zhi, Y.; Li, Z.; Feng, X.; Xia, H.; Zhang, Y.; Shi, Z.; Mu, Y.; Liu, X. Covalent Organic Frameworks as Metal-Free Heterogeneous Photocatalysts for Organic Transformations. *J. Mater. Chem. A* **2017,** *5*, 22933–22938.

49. Wei, P.-F.; Qi, M.-Z.; Wang, Z.-P.; Ding, S.-Y.; Yu, W.; Liu, Q.; Wang, L.-K.; Wang, H.-Z.; An, W.-K.; Wang, W. Benzoxazole-Linked Ultrastable Covalent Organic Frameworks for Photocatalysis. *J. Am. Chem. Soc.* **2018,** *140*, 4623–4631.

50. Kang, X.; Wu, X.; Han, X.; Yuan, C.; Liu, Y.; Cui, Y. Rational Synthesis of Interpenetrated 3D Covalent Organic Frameworks for Asymmetric Photocatalysis. *Chem. Sci.* **2020,** *11*, 1494–1502.

51. Tian, M.; Liu, S.; Bu, X.; Yu, J.; Yang, X. Covalent Organic Frameworks: A Sustainable Photocatalyst toward Visible-Light-Accelerated C_3 Arylation and Alkylation of Quinoxalin-2(1H)-ones. *Chem.–Eur. J.* **2020,** *26*, 369–373.

52. Meng, Y.; Luo, Y.; Shi, J. L.; Ding, H.; Lang, X.; Chen, W.; Zheng, A.; Sun, J.; Wang, C. 2D and 3D Porphyrinic Covalent Organic Frameworks: The Influence of Dimensionality on Functionality. *Angew. Chem., Int. Ed.* **2020,** *59*, 3624–3629.

53. Huang, W.; Ma, B. C.; Lu, H.; Li, R.; Wang, L.; Landfester, K.; Zhang, K. A. I. Visible-Light-Promoted Selective Oxidation of Alcohols Using a Covalent Triazine Framework. *ACS Catal.* **2017,** *7*, 5438–5442.

54. Jin, E.; Li, J.; Geng, K.; Jiang, Q.; Xu, H.; Xu, Q.; Jiang, D. Designed Synthesis of Stable Light-Emitting Two-Dimensional sp^2 Carbon-Conjugated Covalent Organic Frameworks. *Nat. Commun.* **2018,** *9*, 4143.

55. Jadhav, T.; Fang, Y.; Patterson, W.; Liu, C.-H.; Hamzehpoor, E.; Perepichka, D. F. 2D Poly(arylene vinylene) Covalent Organic Frameworks via Aldol Condensation of Trimethyltriazine. *Angew. Chem., Int. Ed.* **2019,** *58*, 13753–13757.

56. Xu, S.; Wang, G.; Biswal, B. P.; Addicoat, M.; Paasch, S.; Sheng, W.; Zhuang, X.; Brunner, E.; Heine, T.; Berger, R.; Feng, X. A Nitrogen-Rich 2D sp^2-Carbon-Linked Conjugated Polymer Framework as a High-Performance Cathode for Lithium-Ion Batteries. *Angew. Chem., Int. Ed.* **2019,** *58*, 849–853.

57. Zhuang, X.; Zhao, W.; Zhang, F.; Cao, Y.; Liu, F.; Bi, S.; Feng, X. A Two-Dimensional Conjugated Polymer Framework with Fully sp^2-Bonded Carbon Skeleton. *Polymer Chemistry* **2016,** *7*, 4176–4181.

58. Jin, E.; Asada, M.; Xu, Q.; Dalapati, S.; Addicoat, M. A.; Brady, M. A.; Xu, H.; Nakamura, T.; Heine, T.; Chen, Q.; Jiang, D. Two-Dimensional sp^2 Carbon-Conjugated Covalent Organic Frameworks. *Science* **2017,** *357*, 673–676.

59. Lyu, H.; Diercks, C. S.; Zhu, C.; Yaghi, O. M. Porous Crystalline Olefin-Linked Covalent Organic Frameworks. *J. Am. Chem. Soc.* **2019,** *141*, 6848–6852.

60. Cui, W. R.; Zhang, C. R.; Jiang, W.; Li, F. F.; Liang, R. P.; Liu, J.; Qiu, J. D. Regenerable and Stable sp^2 Carbon-Conjugated Covalent Organic Frameworks for Selective Detection and Extraction of Uranium. *Nat. Commun.* **2020,** *11*, 436.

61. Jin, E.; Lan, Z.; Jiang, Q.; Geng, K.; Li, G.; Wang, X.; Jiang, D. 2D sp^2 Carbon-Conjugated Covalent Organic Frameworks for Photocatalytic Hydrogen Production from Water. *Chem* **2019,** *5*, 1632–1647.

62. Wei, S.; Zhang, F.; Zhang, W.; Qiang, P.; Yu, K.; Fu, X.; Wu, D.; Bi, S.; Zhang, F. Semiconducting 2D Triazine-Cored Covalent Organic Frameworks with Unsubstituted Olefin Linkages. *J. Am. Chem. Soc.* **2019,** *141*, 14272–14279.

63. Bi, S.; Yang, C.; Zhang, W.; Xu, J.; Liu, L.; Wu, D.; Wang, X.; Han, Y.; Liang, Q.; Zhang, F. Two-Dimensional Semiconducting Covalent Organic Frameworks via Condensation at Arylmethyl Carbon Atoms. *Nat. Commun.* **2019,** *10*, 2467.

64. Chen, R.; Shi, J. L.; Ma, Y.; Lin, G.; Lang, X.; Wang, C. Designed Synthesis of a 2D Porphyrin-Based sp^2 Carbon-Conjugated Covalent Organic Framework for Heterogeneous Photocatalysis. *Angew. Chem., Int. Ed.* **2019,** *58*, 6430–6434.

65. Zhao, Y.; Liu, H.; Wu, C.; Zhang, Z.; Pan, Q.; Hu, F.; Wang, R.; Li, P.; Huang, X.; Li, Z. Fully Conjugated Two-Dimensional sp^2-Carbon Covalent Organic Frameworks as Artificial Photosystem I with High Efficiency. *Angew. Chem., Int. Ed.* **2019,** *58*, 5376–5381.

66. Fu, Z. W.; Wang, X. Y.; Gardner, A.; Wang, X.; Chong, S. Y.; Neri, G.; Cowan, A. J.; Liu, L. J.; Li, X. B.; Vogel, A.; Clowes, R.; Bilton, M.; Chen, L. J.; Sprick, R. S.; Cooper, A. I. A Stable Covalent Organic Framework for Photocatalytic Carbon Dioxide Reduction. *Chem. Sci.* **2020,** *11*, 543–550.

67. Luo, J.; Lu, J.; Zhang, J. Carbazole–Triazine Based Donor–Acceptor Porous Organic Frameworks for Efficient Visible-Light Photocatalytic Aerobic Oxidation Reactions. *J. Mater. Chem. A* **2018,** *6*, 15154–15161.

68. Ou, W.; Zhang, G.; Wu, J.; Su, C. Photocatalytic Cascade Radical Cyclization Approach to Bioactive Indoline-Alkaloids over Donor–Acceptor Type Conjugated Microporous Polymer. *ACS Catal.* **2019,** *9*, 5178–5183.

69. Liu, G.; Zhao, G.; Zhou, W.; Liu, Y.; Pang, H.; Zhang, H.; Hao, D.; Meng, X.; Li, P.; Kako, T.; Ye, J. In Situ Bond Modulation of Graphitic Carbon Nitride to Construct p-n Homojunctions for Enhanced Photocatalytic Hydrogen Production. *Adv. Funct. Mater.* **2016,** *26*, 6822–6829.

70. Nosaka, Y.; Nosaka, A. Y. Generation and Detection of Reactive Oxygen Species in Photocatalysis. *Chem. Rev.* **2017,** *117*, 11302–11336.

71. Xie, J. H.; Zhu, S. F.; Zhou, Q. L. Transition Metal-Catalyzed Enantioselective Hydrogenation of Enamines and Imines. *Chem. Rev.* **2011,** *111*, 1713–1760.

72. Kang, N.; Park, J. H.; Ko, K. C.; Chun, J.; Kim, E.; Shin, H. W.; Lee, S. M. Kim, H. J.; Ahn, T. K.; Lee, J. Y.; Son, S. U. Tandem Synthesis of Photoactive Benzodifuran Moieties in the Formation of Microporous Organic Networks. *Angew. Chem., Int. Ed.* **2013,** *52*, 6228–6232.

73. Chen, P.; Guo, Z.; Liu, X.; Lv, H.; Che, Y.; Bai, R.; Chi, Y.; Xing, H. A Visible-Light-Responsive Metal–Organic Framework for Highly Efficient and Selective Photocatalytic Oxidation of Amines and Reduction of Nitroaromatics. *J. Mater. Chem. A* **2019,** *7*, 27074–27080.

74. Wei, H.; Guo, Z.; Liang, X.; Chen, P.; Liu, H.; Xing, H. Selective Photooxidation of Amines and Sulfides Triggered by a Superoxide Radical Using a Novel Visible-Light-Responsive Metal-Organic Framework. *ACS Appl. Mater. Interfaces* **2019,** *11*, 3016–3023.

75. Su, C.; Tandiana, R.; Tian, B.; Sengupta, A. Tang, W.; Su, J.; Loh, K. P. Visible-Light Photocatalysis of Aerobic Oxidation Reactions Using Carbazolic Conjugated Microporous Polymers. *ACS Catal.* **2016,** *6*, 3594–3599.

76. Liu, Z.; Su, Q.; Ju, P.; Li, X.; Li, G.; Wu, Q.; Yang, B. A Hydrophilic Covalent Organic Framework for Photocatalytic Oxidation of Benzylamine In Water. *Chem. Commun.* **2020,** *56*, 766–769.

77. Martinez, A.; Alonso, M.; Castro, A.; Perez, C.; Moreno, F. J. First Non-ATP Competitive Glycogen Synthase Kinase 3β (GSK-3β) Inhibitors: Thiadiazolidinones (TDZD) as Potential Drugs for the Treatment of Alzheimer's Disease. *J. Med. Chem.* **2002,** *45*, 1292–1299.

78. Iizawa, Y.; Okonogi, K.; Hayashi, R.; Iwahi, T.; Yamazaki, T.; Imada, A. Therapeutic Effect of Cefozopran (SCE-2787), a New Parenteral Cephalosporin, Against Experimental Infections in Mice. *Antimicrob. Agents Chemother.* **1993,** *37*, 100–105.

79. Cheng, D.; Luo, R.; Zheng, W.; Yan, J. Highly Efficient Oxidative Dimerization of Thioamides to 3,5-Disubstituted 1,2,4-Thiadiazoles Mediated by DDQ. *Synthetic Comm*. **2012,** *42*, 2007–2013.

80. Shah, A. U.; Khan, Z. A.; Choudhary, N.; Loholter, C.; Schafer, S.; Marie, G. P.; Farooq, U.; Witulski, B.; Wirth, T. Iodoxolone-Based Hypervalent Iodine Reagents. *Org. Lett*. **2009,** *11*, 3578–3581.

81. Yajima, K.; Yamaguchi, K.; Mizuno, N. Facile Access to 3,5-Symmetrically Disubstituted 1,2,4-Thiadiazoles through Phosphovanadomolybdic Acid Catalyzed Aerobic Oxidative Dimerization of Primary Thioamides. *Chem. Commun*. **2014,** *50*, 6748–6750.

82. Yadav, L.; Srivastava, V.; Yadav, A. Eosin Y Catalyzed Visible-Light-Driven Aerobic Oxidative Cyclization of Thioamides to 1,2,4-Thiadiazoles. *Synlett* **2013,** *24*, 465–470.

83. Lang, X.; Ji, H.; Chen, C.; Ma, W.; Zhao, J. Selective Formation of Imines by Aerobic Photocatalytic Oxidation of Amines on TiO_2. *Angew. Chem., Int. Ed*. **2011,** *50*, 3934–3937.

84. Su, C.; Acik, M.; Takai, K.; Lu, J.; Hao, S. J.; Zheng, Y.; Wu, P.; Bao, Q.; Enoki, T.; Chabal, Y. J.; Loh, K. P. Probing the Catalytic Activity of Porous Graphene Oxide and the Origin of This Behaviour. *Nat. Commun*. **2012,** *3*, 1298.

85. Su, F.; Mathew, S. C.; Mohlmann, L.; Antonietti, M.; Wang, X.; Blechert, S. Aerobic Oxidative Coupling of Amines by Carbon Nitride Photocatalysis with Visible Light. *Angew. Chem., Int. Ed*. **2011,** *50*, 657–660.

86. Vanajatha, G.; Reddy, V. P. High Yielding Protocol for Oxidative Dimerization of Primary Thioamides: A Strategy toward 3,5-Disubstituted 1,2,4-Thiadiazoles. *Tetrahedron Letters* **2016,** *57*, 2356–2359.

87. Wang, Z. Q.; Meng, X. J.; Li, Q. Y.; Tang, H. T.; Wang, H. S.; Pan, Y. M. Electrochemical Synthesis of 3,5-Disubstituted-1,2,4-thiadiazoles through NH_4I-Mediated Dimerization of Thioamides. *Advanced Synthesis & Catalysis* **2018,** *360*, 4043–4048.

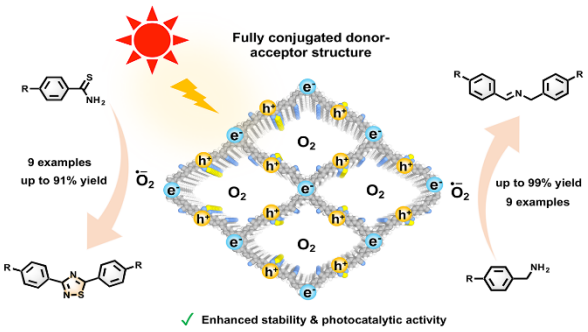

TOC (3.25 inches × 1.75 inches)

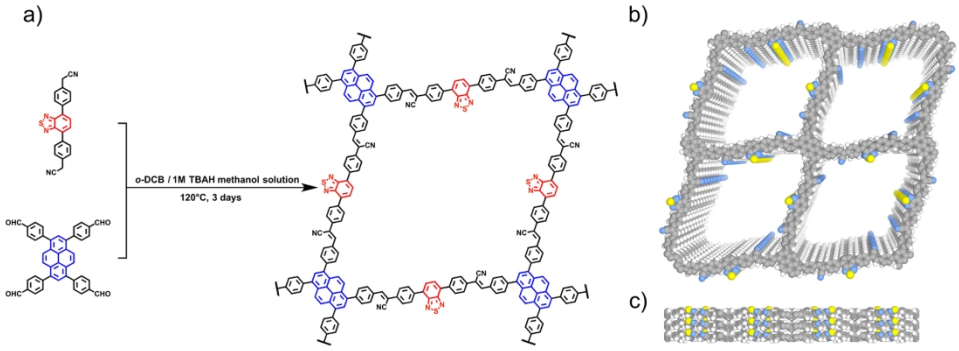

Figure 1. a) The synthetic condition of Py-BSZ-COF. b) Top and c) side views of the structural model of Py-BSZ-COF (C, gray; N, blue; S, yellow; H, white).

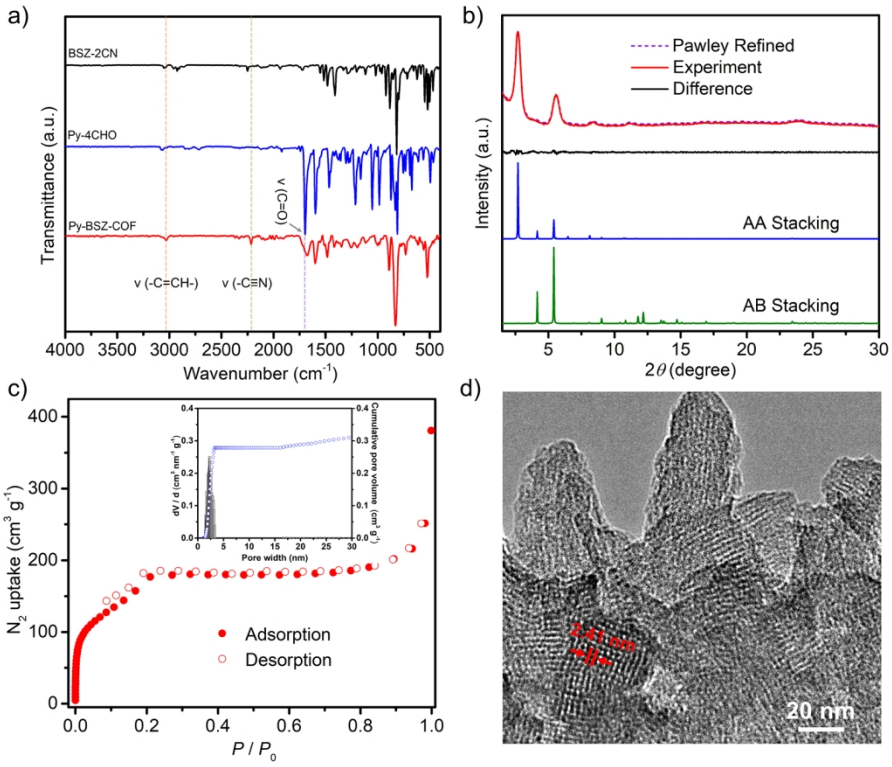

Figure 2. a) FT-IR spectra of Py-BSZ-COF, BSZ-2CN and Py-4CHO. b) Experimentally observed PXRD pattern, Pawley refinement and their difference of Py-BSZ-COF (red, purple dots, black), the simulated PXRD patterns of the AA stacking model (blue) and the AB stacking model (green). c) N2 isotherm of Py-BSZ-COF at 77 K, inset: pore width distribution and cumulative pore volume of Py-BSZ-COF by NLDFT. d) HR-TEM image of Py-BSZ-COF.

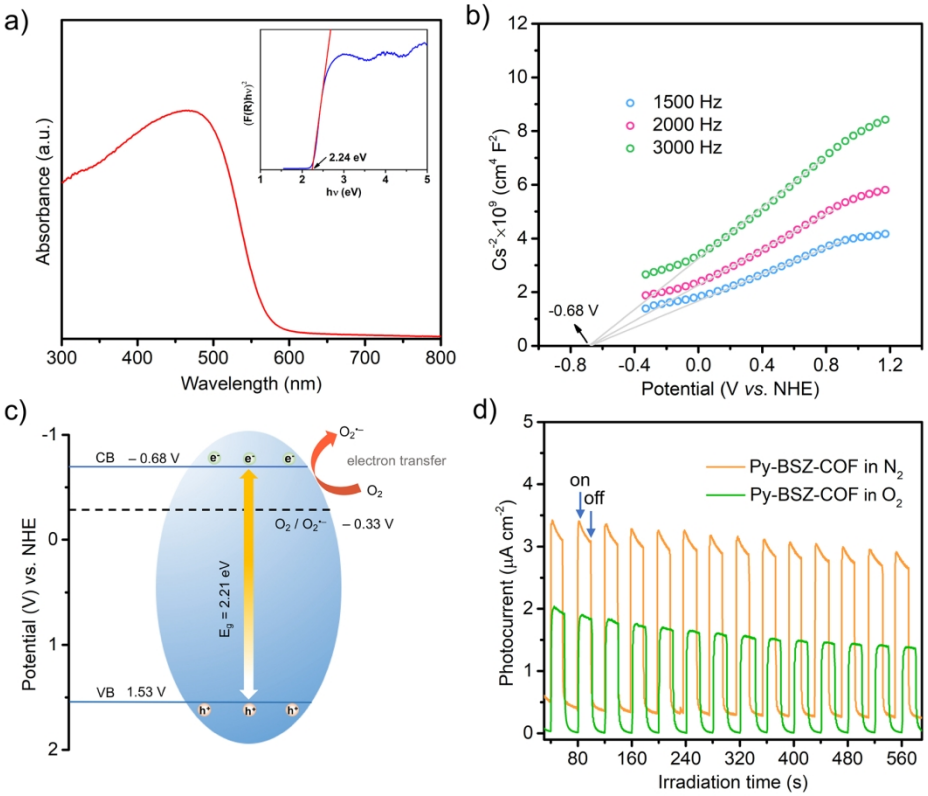

Figure 3. a) Solid state UV−vis diffuse reflectance spectra (red), inset: Tauc plot of Py-BSZ-COF (blue). b) The Mott-Schottky plots of Py-BSZ-COF. c) The band energy diagram of Py-BSZ-COF. d) Photocurrent responses spectra of Py-BSZ-COF under nitrogen or oxygen atmosphere.

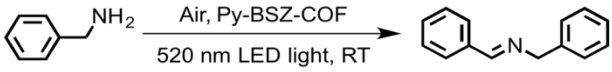

Entry	Reaction condition variations	Light	Conversion[b](%)
1	–	on	99
2[c]	–	off	4
3[d]	no O_2	on	9
4	no photocatalyst	on	5
5[e]	L-histidine	on	94
6[f]	catalase	on	96
7[g]	isopropanol	on	95
8[h]	*p*-benzoquinone	on	28
9[i]	$AgNO_3$	on	1
10[j]	KI	on	38
11	sp^2c-COF-3	on	67
12	COF-JLU22	on	90[k]

Table 1. Control experiments of the photocatalytic oxidative amine coupling of benzylamine.

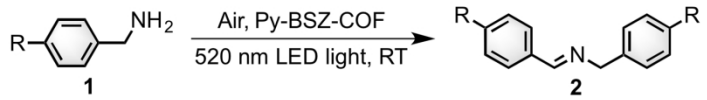

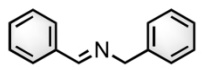

2a

12 h, 99%, 99%

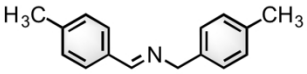

2b

12 h, 99%, 99%

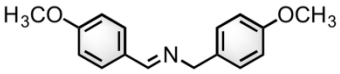

2c

12 h, 98%, 99%

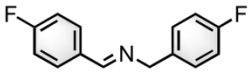

2d

12 h, 99%, 99%

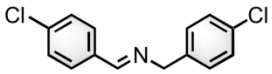

2e

12 h, 99%, 99%

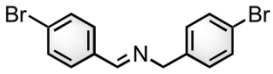

2f

12 h, 99%, 99%

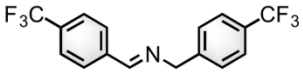

2g

12 h, 98%, 98%

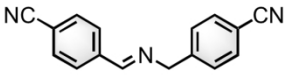

2h

12 h, 52%, 99%

24 h, 84%, 99%

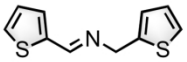

2i

12 h, 67%, 99%

24 h, 99%, 99%

Table 2. Heterogeneous photocatalytic oxidative coupling of diverse amines.

177x126mm (300 x 300 DPI)

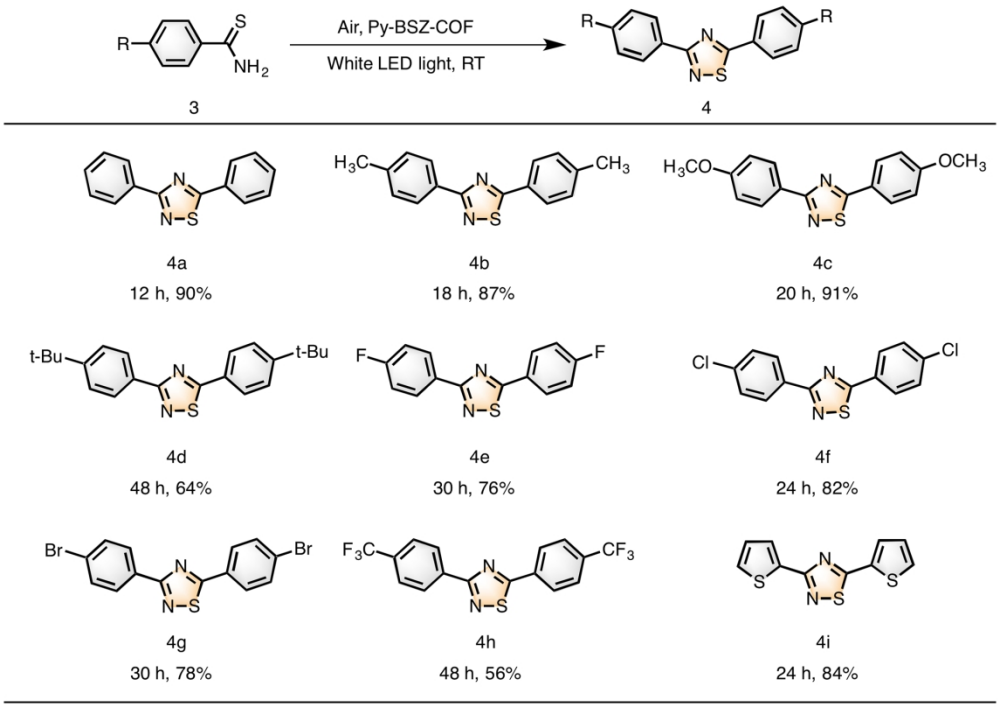

Table 3. Heterogeneous photocatalytic oxidative cyclization of diverse thioamides to 1,2,4-thiadiazoles.

177x125mm (300 x 300 DPI)

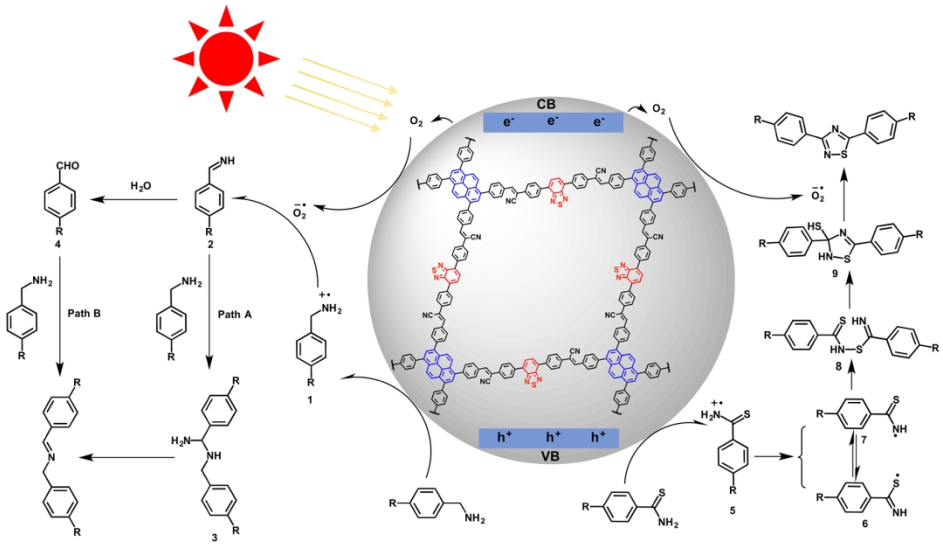

Figure 4. The plausible photocatalytic mechanisms of Py-BSZ-COF mediated oxidative amine coupling and cyclization of thioamide to 1,2,4-thiadiazole.